FMC

A program to manage, classify and plot focal mechanism data

VERSION 1.3, OCTOBER 2018

José A. Álvarez-Gómez

Faculty of Geology. Universidad Complutense de Madrid

Contents

Acknowledgments

I have been using different versions of this program during the last decade. Initially I reworked some of the Gasperini and Vannucci (2003) FORTRAN subroutines on Matlab in order to obtain all the focal mechanism parameters from the Harvard CMT `psmeca` formatted catalog. During my research on seismotectonics I started to use the Frohlich and Apperson (1992) diagram, but after Kagan (2005) I decided to try the Kaverina et al. (1996) one. From the original Matlab program I jumped to the Free Software world adapting it to Octave. The program only produced the x and y positions of the events and all the plotting was done by means of GMT (Wessel et al., 2013).

Some colleagues wanted to use the diagram for their work, but they were not familiar with GMT, so I decided to make a big improvement in the program to make it easy to use, distributable and with plotting support. I choose to program it in Python with the following basic ideas:

1. It should be called from the terminal or the command line in order to be incorporated into shell scripts

2. It should behave like any other shell unix tool, compatible with redirection, piping and ASCII format

3. it should be compatible with the GMT `psmeca` formats to allow the mapping of the focal mechanisms

4. It should has the option to produce a Kaverina et al. (1996) type classification diagram

Part of the programming was done during my happy days as Ph.D. candidate at the UCM; so I have to acknowledge the UCM scholarship that allowed me to start my scientific career.

I would like to thank the beta testers Jorge L. Giner-Robles and Alberto Jiménez-Díaz for their comments and suggestions. Dr. Andrei Bala (National Institute for Earth Physics, Romania) has tested different versions and suggested several improvements.

If you use `FMC`, and consider it appropriate, you can acknowledge it by citing the following reference:

- Álvarez-Gómez, J.A. (2014) FMC: a one-liner Python program to manage, classify and plot focal mechanisms. Geophysical Research Abstracts, Vol. 16, EGU2014-10887.

Part I

The manual

1 Introduction

This is the user manual for the program `FMC` (from Focal Mechanisms Classification). This program was originally developed on Python 2.7.3 and adapts some of the Gasperini and Vannucci (2003) FORTRAN routines to obtain the different parameters of the earthquake focal mechanisms depending on the input format. Since version 1.3 it is compatible with Python 3. Several output formats are eligible, clustering analysis of the data can be performed and a classification diagram for the focal mechanisms is produced. The default input and output formats are the same used by the GMT program `psmeca` in order to make the program integration easiest and facilitate the mapping of the data.

The program basically takes the focal mechanisms data, computes the different parameters that can be obtained, classifies each focal mechanism in one of seven possible types, perform a clustering analysis of the data if it is required by the user and optionally outputs the parameters in different formats and generates a classification diagram from the input data.

2 Versions

1.3 New features:

- Added support for Pyhton 3

- Added new base diagram labels and tick marks.

- Added symbol labeling.

1.2 New features:

- Added slip sense and plunge parameters for each focal mechanism nodal plane.

1.1 New features:

- New custom output parsing. The user can choose between the standard predefined output or any parameters in any order.

- Added a header with the parameter name in the output.

- Added symbol coloring.

- Added hierarchical clustering with several methods and options.

1.01   New features:

- Column number is now included in the header of the output file with all the parameters.

Bug fixes:

- Error in the nd2ar function to obtain the tensor components from the nodal planes.

1.0   Initial release of `FMC` with basic plotting function and focal mechanims management.

3   Installation

`FMC` has been programmed in Python 2.7.3 and uses several common python libraries: `sys`, `argparse`, `os`, `NumPy` and `matplotlib`. Depending on your operative system and Python installation you could need to install some of the libraries manually.

Since version 1.3 `FMC` works also on Python 3. In order to work properly `FMC` needs `NumPy` version 1.14 or higher.

For **Windows** and **Mac** users a good starting point is the installation of predefined packages. From www.SciPy.org you can download program packages that includes `Python`, `NumPy` and `matplotlib`, as well as other modules and IDEs. With one of these packages installed `FMC` should work properly.

For **Linux** users all the required software can be easily installed through your favorite distribution repository (the python modules `sys`, `argparse` and `os` are usually installed with the default python installation).

4   Usage

The user interface is as simple as a "command line", or a "terminal". I decided to keep the program as simple as possible so it can be integrated into

scripts with other programs such as GMT, `AWK (or gawk)` or any other tool running from a shell or script (in *nix) or a command window or batch file (in Windows/DOS). In the following the commands are written assuming that your python installation recognizes automatically the python format. In some systems, depending on your personal configuration, you will need to call first Python (like "`python FMC.py...`" or "`python3 FMC.py...`") or in a *nix system with the "`./`" needed to execute a script (like `./FMC.py ...`).

In *nix you will need to give execution permission to the program:

```
chmod +x FMC.py
```

To run `FMC` on a file simply type in the terminal:

```
FMC.py input-file.dat
```

By default `FMC` will read the input file as a `psmeca` Centroid Moment Tensor (CMT) format (in Harvard convention). This kind of file can be downloaded directly from Global CMT. The output will be shown on the screen in `psmeca` CMT format so it can be directly pipe into `psmeca`:

```
FMC.py input-file.dat | psmeca -R {...etc}
```

Or stored as an ASCII file:

```
FMC.py input-file.dat > output-file.dat
```

In this case `FMC` will add a new column at the end of each register with the focal mechanism type.

Alternatively the input file can be a single plane in Aki and Richards (1980) convention (Right Hand Rule for the plane orientation, and rakes from 0 to 180 in reverse faults and 0 to -180 in normal faults, 0 for left-lateral and ±180 for right-lateral). This format is also compatible with `psmeca`.

4.1 Input

`FMC` input can be given as an ASCII file or as standard input, from a pipe ("|") or a redirection ("<"). The following codes are then equivalent:

```
FMC.py input-file.dat
cat input-file.dat | FMC.py
FMC.py < input-file.dat
```

If no input is given, then `FMC` will show the on-screen help.

The input format is specified with the optional flag "-i", and the possible values are:

CMT Harvard Centroid Moment Tensor (by default):
   `[longitude, latitude, depth, mrr, mtt, mff, mrt, mrf, mtf, Exponent (dyn-cm), X plot, Y plot (for GMT), ID]`

AR Aki and Richards one plane convention:
   `[longitude, latitude, depth, strike, dip, rake, magnitude (Mw), X plot, Y plot (for GMT), ID]`

4.2 output

`FMC` output format can be selected among the following options with the flag "-o":

CMT Harvard Centroid Moment Tensor (`psmeca` compatible):
   `[longitude, latitude, depth, mrr, mtt, mff, mrt, mrf, mtf, Exponent (dyn·cm), X plot, Y plot (for GMT), ID, TYPE]`

P Focal mechanism both nodal planes (`psmeca` compatible):
   `[longitude, latitude, depth, strike A, dip A, rake A, strike B, dip B, rake B, Scalar seismic moment mantissa, Exponent (dyn·cm), X plot, Y plot (for GMT), ID, TYPE]`

AR Focal mechanism one plane (`psmeca` compatible):
   `[longitude, latitude, depth, strike, dip, rake, magnitude (Mw), X plot, Y plot (for GMT), ID, TYPE]`

K Kaverina diagram position for plotting outside FMC:
   `[X Kaverina diagram, Y Kaverina diagram, Mw, Depth, ID, TYPE]`

ALL All the parameters obtained:
   `[longitude, latitude, depth, mrr, mtt, mff, mrt, mrf, mtf, Exponent (dyn·cm), Scalar seismic moment (dyn·cm), Mw, strike A, dip A, rake A, strike B, dip B, rake B, Slip trend A, Slip plunge A, Slip trend B, Slip plunge B, P trend, P plunge, B trend, B plunge, T trend, T plunge, fclvd, X Kaverina diagram, Y Kaverina diagram, ID, TYPE]`

CUSTOM In case you need any focal mechanism parameters in any order you can use the CUSTOM option and give the requested parameters in any order using the flag "-of". The output parameters need to be listed separated by commas. The accepted parameters names are listed below, and can be seen on the terminal using `FMC.py -helpFields`

lon longitude

lat latitude

dep depth

mrr mrr centroid moment tensor component

mtt mtt centroid moment tensor component

mff mff centroid moment tensor component

mrt mrt centroid moment tensor component

mrf mrf centroid moment tensor component

mtf mtf centroid moment tensor component

mant mantissa of the seismic moment tensor

expo exponent of the seismic moment tensor

Mo Scalar seismic moment

Mw Moment (or Kanamori) magnitude

strA Strike of nodal plane A

dipA Dip of nodal plane A

rakeA Rake of nodal plane A

strB Strike of nodal plane B

dipB Dip of nodal plane B

rakeB Rake of nodal plane B

slipA Slip sense of plane A

plungA Plunge of slip vector of plane A

slipB Slip sense of plane B

plungB Plunge of slip vector of plane B

trendp Trend of P axis

plungp Plunge of P axis

trendb Trend of B axis

plungb Plunge of B axis

trendt Trend of T axis

plungt Plunge of T axis

fclvd Compensated linear vector dipole ratio

x_kav x position on the Kaverina diagram

y_kav y position on the Kaverina diagram

ID ID of the event

clas Focal mechanism rupture type

posX X plotting position for GMT psmeca

posY Y plotting position for GMT psmeca

Examples of use

Obtaining nodal planes from moment tensor

Command:

```
echo -2.54 37.09 12 -3.4669 -2.0652 5.5321 6.2368 -1.8004 -5.1775 22 X Y ID | FMC.py -o P
```

Result:

```
#Longitude Latitude Depth_(km) Strike_A Dip_A Rake_A Strike_B Dip_B Rake_B Seismic_moment_mantissa
Exponent_(dyn-cm) X_position(GMT) Y_position(GMT) ID Rupture_type
-2.54 37.09 12.0 190.925 42.4899 -20.9735 296.709 76.0089 -130.541 9.6045 22.0 X Y ID N-SS
```

Obtaining moment tensor from one nodal plane

Command:

```
echo -2.54 37.09 12 190.925 42.4899 -20.9735 4.6 X Y ID | FMC.py -i AR -o CMT
```

Result:

```
#Longitude Latitude Depth_(km) mrr mtt mff mrt mrf mtf Exponent_(dyn-cm) X_position(GMT) Y_position(GMT) ID
Rupture_type
-2.54 37.09 12.0 -3.56563 -2.21928 5.78491 6.70126 -1.61249 -5.19047 22.0 X Y ID N-SS
```

Obtaining all the parameters from the moment tensor

Command:

```
echo -2.54 37.09 12 -3.4669 -2.0652 5.5321 6.2368 -1.8004 -5.1775 22 X Y ID | FMC.py -o ALL
```

Result:

```
#Longitude Latitude Depth_(km) mrr mtt mff mrt mrf mtf Exponent_(dyn-cm) Seismic_moment_Mo Magnitude_Mw Strike_A
Dip_A Rake_A Strike_B Dip_B Rake_B Slip_trend_A Slip_plunge_A Slip_trend_B Slip_plunge_B Trend_P Plunge_P
Trend_B Plunge_B Trend_T Plunge_T fclvd X_Kaverina Y_Kaverina ID Rupture_type
-2.54 37.09 12.0 -3.4669 -2.0652 5.5321 6.2368 -1.8004 -5.1775 22.0 9.6045e+22 4.6 190.925 42.4899 -20.9735
296.709 76.0089 -130.541 206.709 -13.9911 100.925 -47.5101 167.141 43.8185 308.393 39.1024 56.0979 20.5155
0.0445259 -0.243839 0.0899979 ID N-SS
```

Obtaining all the parameters from CMT input file and storing to an ASCII file

Command:

```
FMC.py -o ALL japan_CMT.dat > Japan_parameters.dat
```

Using CUSTOM output to obtain event location and slip vector of both nodal planes

Command:

```
echo -2.54 37.09 12 -3.4669 -2.0652 5.5321 6.2368 -1.8004 -5.1775 22 X Y ID | FMC.py -o CUSTOM -of

lon,lat,slipA,plungA,slipB,plungB
```

Result:

```
#Longitude Latitude Slip_trend_A Slip_plunge_A Slip_trend_B Slip_plunge_B
2.54 37.09 206.709 -13.9911 100.925 -47.5101
```

4.3 Plot

Optionally `FMC` will produce a classification diagram. `FMC` uses `matplotlib` libraries and can generate figures in different formats (emf, eps, jpeg, jpg, pdf, png, ps, raw, rgba, svg, svgz, tif, tiff). The format is determined automatically from the plot file name extension.

The diagram uses the Kaverina et al. (1996) projection technique, used also by Kagan (2005); but incorporating a classification similar to the geological conceptual classification of faults. The earthquakes are classified into seven types according to the values of the P, T and B Centroid Moment Tensor axes following a simple algorithm (Figure 4.1), and are represented conveniently on the Kaverina diagram (Figure 4.2). This classification is very similar to the used by Johnston et al. (1994).
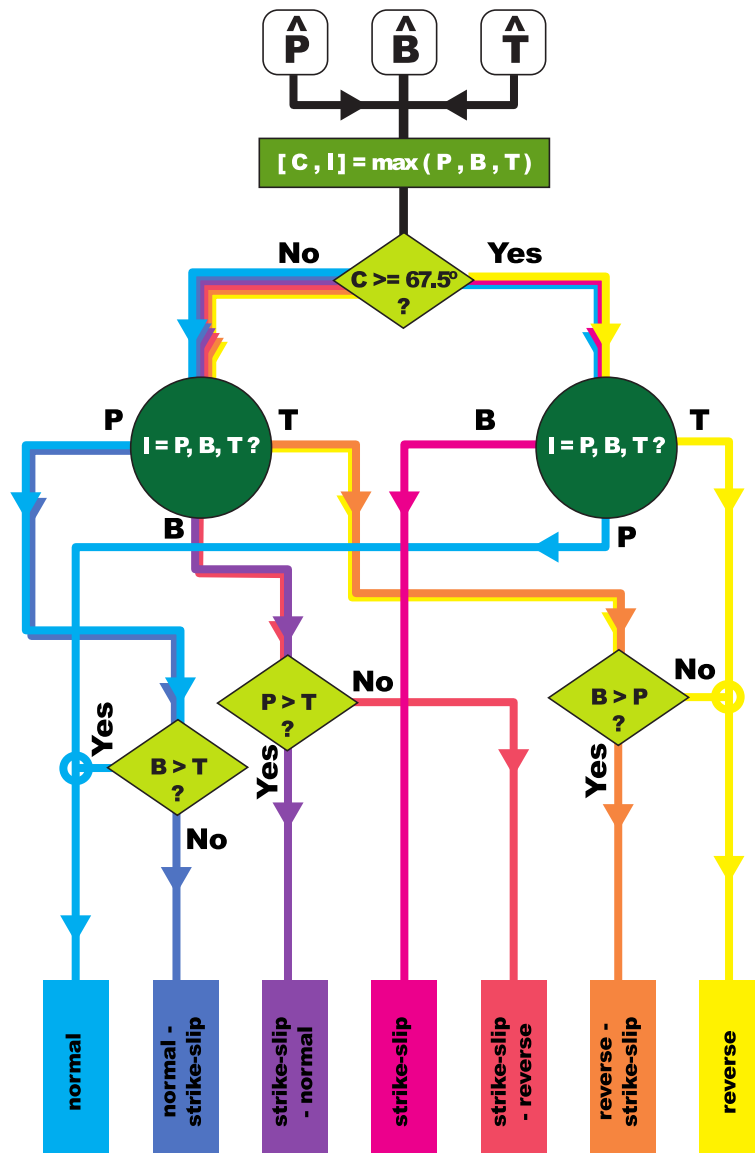
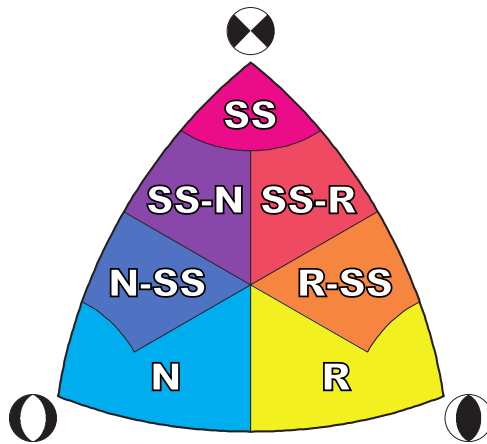Figure 4.1: Focal mechanism classification algorithm flow chart.

Figure 4.2: Classification diagram. N: Normal; N-SS: Normal - Strike-slip; SS-N: Strike-slip - Normal; SS: Strike-slip; SS-R: Strike-slip - Reverse; R-SS: Reverse - Strike-slip; R: Reverse.

`FMC` uses several flags in order to customize the plot.

-p This flag activates the plotting. It must be followed by the name of the figure file that will be produced. The name used for the file (without the extension) is used as title for the plot.

-pc With this flag the user specifies the parameter that is used to fill the symbols. A color palette is produced with the range of the selected parameter values.

-a This flag is used to annotate the symbols with a certain parameter.

With -pc and -a the parameters must be given with its corresponding internal name as listed in section .

Examples of use

Plotting data from standard input

Command:

```
echo -2.54 37.09 12 -3.4669 -2.0652 5.5321 6.2368 -1.8004 -5.1775 22 X Y ID | FMC.py -p "My data.png"
```
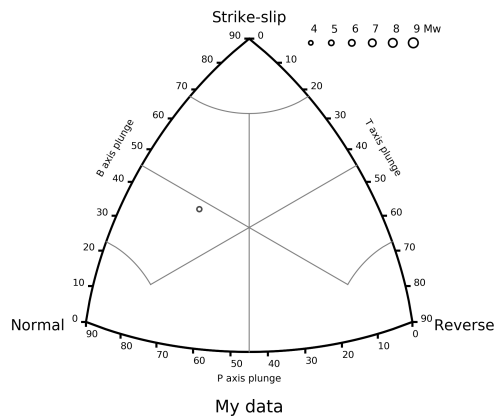
My data

Figure 4.3: Plot result from the command "`echo -2.54 37.09 12 -3.4669 -2.0652 5.5321 6.2368 -1.8004 -5.1775 22 X Y ID | FMC.py -p` "My data.png""

Plotting data from input file and shading the symbols with a parameter

Command:

```
FMC.py -p 'Japan 2011 data.png' japan_CMT_2011.dat -pc fclvd
```
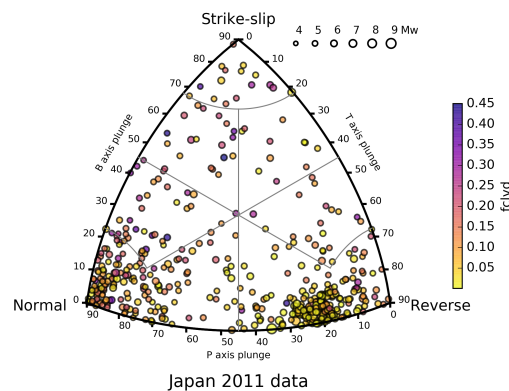

Japan 2011 data

Figure 4.4: Plot result from the command "`FMC.py -p 'Japan 2011 data.png' japan_CMT_2011.dat -pc fclvd`"

Plotting data from input file shading and annotating the symbols

Command:

```
FMC.py Japan_CMT_2011_biggest.dat -p "Japan 2011 biggest events.png" -pc dep -a Mw
```
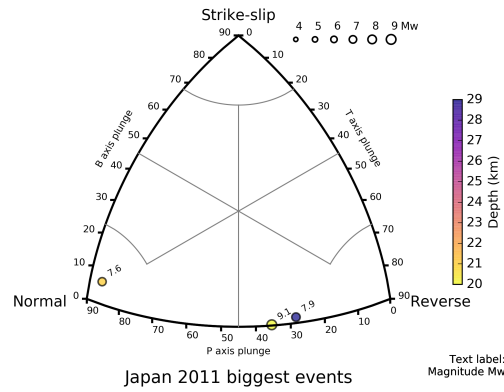
Figure 4.5: Plot result from the command "`FMC.py Japan_CMT_2011_biggest.dat -p "Japan 2011 biggest events.png" -pc dep -a Mw`"

Plotting data from input file and piping to psmeca

Command:

```
FMC.py -p 'Japan data.pdf' japan_CMT.dat | psmeca -R125/170/30/60 -JM8c -Ba10f2WESN -Sm5p/-1 > CMT_map.ps
```
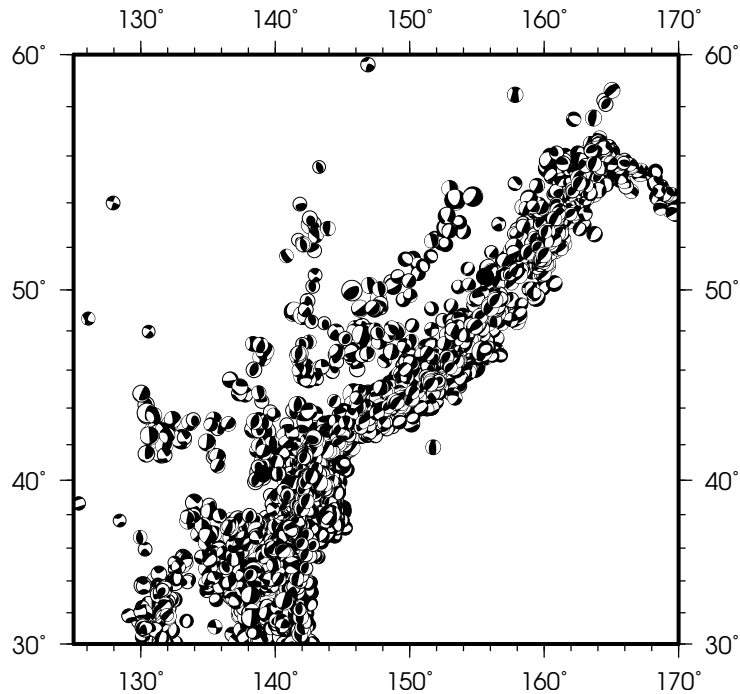

Figure 4.6: Map generated with `psmeca` (GMT) from the `FMC` output.

4.4 Clustering

`FMC` implements the hierarchical agglomerative clustering algorithms from SciPy (scipy.cluster.hierarchy) in order to group the data[1] . The advantages of this algorithms are its versatility, as the user can choose between a number of metrics and grouping methods, its capacity to automatically select a minimum number of clusters without an a priori estimation, and its potential to work with different parameters with different scales and with strong different populations in clusters.

The parameters for the clustering are passed by several optional flags. If any of the following flags is given in the command line `FMC` will perform the clustering analysis using some default options if needed. When a clustering analysis is done, by default `FMC` will shade the symbols in the diagram using the cluster number, unless a different parameter is stated with `-pc` flag.

`-cm` Method to be used in the clustering analysis. The options are:

single single/min/nearest

$$d(u,v) = \min(dist(u\,[i]\,,v\,[j]))$$

complete complete/max/farthest point

$$d(u,v) = \max(dist(u\,[i]\,,v\,[j]))$$

average average/UPGMA

$$d(u,v) = \sum_{ij} \frac{d(u\,[i]\,,v\,[j])}{(|u| * |v|)}$$

weighted weighted/WPGMA

$$d(u,v) = (dist(s,v) + dist(t,v))/2$$

centroid centroid/UPGMC [default]

$$dist(s,t) = \|c_s - c_t\|_2$$

where c_s and c_t are the centroids of clusters s and t, respectively. When two clusters s and t are combined into a new cluster u, the new centroid is computed over all the original objects in clusters s and t. The distance then becomes the Euclidean distance between the centroid of u and the centroid of a remaining cluster v in the forest.

---

[1]The details on the clustering algorithms shown in this section are taken from the SciPy documentation.

median median/WPGMC, assigns $d(s,t)$ like the centroid method. When two clusters s and t are combined into a new cluster u, the average of centroids s and t give the new centroid.

ward Ward variance minimization algorithm.

$$d(u,v) = \sqrt{\frac{|v|+|s|}{T}d(v,s)^2 + \frac{|v|+|t|}{T}d(v,t)^2 - \frac{|v|}{T}d(s,t)^2}$$

where u is the newly joined cluster consisting of clusters s and t, v is an unused cluster in the forest,$T = |v| + |s| + |t|$, and $|*|$ is the cardinality of its argument.

Methods "centroid", "median" and "ward" are correctly defined only if Euclidean pairwise metric is used.

-ce Metric used to measure distances between events parameters. These metrics work with non-Boolean vectors. By default `FMC` uses euclidean distance.

braycurtis The Bray-Curtis distance between two points u and v is

$$d(u,v) = \frac{\sum_i |u_i - v_i|}{\sum_i |u_i + v_i|}$$

canberra The Canberra distance between two points u and v is

$$d(u,v) = \sum_i \frac{|u_i - v_i|}{|u_i| + |v_i|}$$

chebyshev The Chebyshev distance between two n-vectors u and v is the maximum norm-1 distance between their respective elements. More precisely, the distance is given by

$$d(u,v) = \max_i |u_i - v_i|$$

cityblock City block or Manhattan distance between the points.

correlation Correlation distance between vectors u and v. This is

$$1 - \frac{(u - \bar{u}) \cdot (v - \bar{v})}{\|(u - \bar{u})\|_2 \|(v - \bar{v})\|_2}$$

cosine Cosine distance between vectors u and v,

$$1 - \frac{u \cdot v}{\|u\|_2 \|v\|_2}$$

euclidean Distance between m points using Euclidean distance (2-norm). [Default]

hamming Normalized Hamming distance, or the proportion of those vector elements between two n-vectors u and v which disagree.

jaccard Jaccard distance between the points. Given two vectors, u and v, the Jaccard distance is the proportion of those elements $u[i]$ and $v[i]$ that disagree.

mahalanobis The Mahalanobis distance between two points u and v is

$$\sqrt{(u-v)(1/V)(u-v)^T}$$

where $1/V$ is the inverse covariance matrix.

minkowski Distances using the Minkowski distance $\|u-v\|_p$ (p-norm) where $p \geq 1$.

seuclidean Standardized Euclidean distance. The standardized Euclidean distance between two n-vectors u and v is

$$\sqrt{\sum (u_i - v_i)^2 \div V[x_i]}$$

V is the variance vector; $V[i]$ is the variance computed over all the i'th components of the points. It is automatically computed.

sqeuclidean Squared Euclidean distance $\|u-v\|_2^2$ between the vectors.

-cn A priori number of clusters to obtain. If zero or non-present the number of clusters is automatically computed using the Elbow method. This method uses the percentage of variance explained as a function of the number of clusters; when the increment of number of clusters does not improves the percentage of variance explained the number of clusters is set.

-ci Parameters used to perform the cluster analysis. By default `FMC` uses the position on the Kaverina diagram, which is a proxy for the principal moment tensor axes plunges. If the parameters given are not in the same physical magnitude and unit the euclidean distance is not appropriate and a different metric should be used. In these cases the Mahalanobis distance is a good choice, as is equivalent to the Euclidean distance in the transformed space, using the covariance matrix of each parameter.

The parameters must be given with its corresponding internal name as listed in section .

Examples of use

Automatic clustering using the position in the Kaverina diagram (default)

```
FMC.py -p 'Japan 2011 clusters.png' japan_CMT_2011.dat -cn 0
```
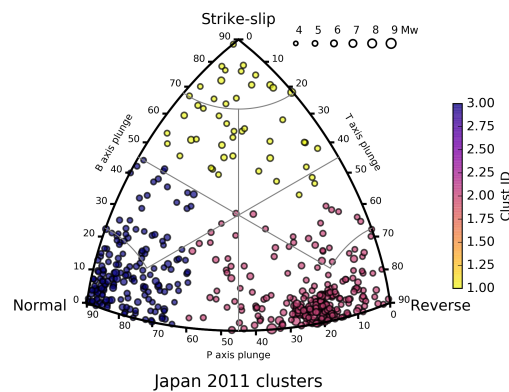

Japan 2011 clusters

Figure 4.7: Plot result from the command ''`FMC.py -p 'Japan 2011 clusters.png' japan_CMT_2011.dat -cn 0`''

Clustering using the epicentral location

```
FMC.py japan_CMT_2011.dat -cn 4 -ci lon,lat
```
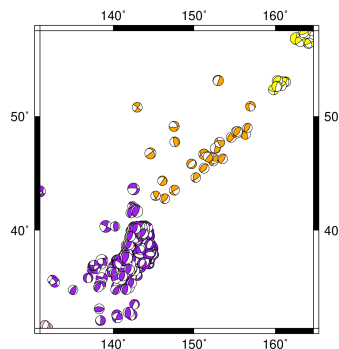

Figure 4.8: Plotting with GMT `psmeca` of the clusters obtained with the command ''`FMC.py -p 'Japan 2011 spatial clusters.png' japan_CMT_2011.dat -cn 4 -ci lon,lat`''

Clustering using Mahalanobis metric and complete grouping with the slip and plunge of the slip vector of nodal plane A

```
FMC.py -p 'Japan 2011 clusters plane A.png' japan_CMT_2011.dat -cn 4 -ci slipA,plungA -cm complete -ce
mahalanobis
```


Japan 2011 clusters plane A

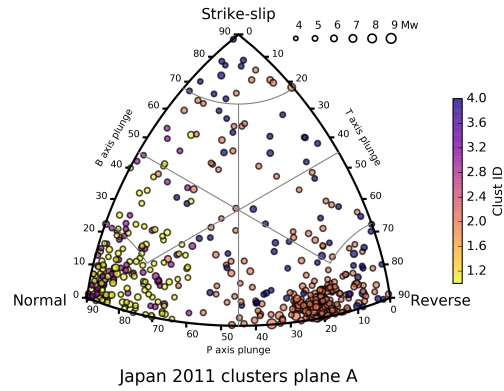Figure 4.9: Plotting with `GMT psmeca` of the clusters obtained with the command "`FMC.py -p 'Japan 2011 clusters plane A.png' japan_CMT_2011.dat -cn 4 -ci slipA,plungA -cm complete -ce mahalanobis`"

5 License

`FMC` has been developed with Free Software and/or Open Source tools. `FMC` uses `NumPy` and `matplotlib` which are distributed under BSD license.

`FMC` is distributed under GNU Generic Public License.

Part II

The background

6 Introduction

Seismicity is frequently used to deduce the tectonics of a region. The study of earthquakes as a tectonic component, the seismotectonics (Scholz, 2002), has grown as one of the key research areas on active tectonics, specially from the analysis of earthquake focal mechanisms.

The first focal mechanism determination methods, based on P wave's first motion polarities, were developed on the first half of the 20th century, specially in Japan where a dense seismic network were available (Byerly, 1928, 1938; Koning, 1941; Honda and Masatuke, 1952; Scheidegger, 1957). Since 1960 the development of the digital computer allow the numerical determination of fault-plane solutions with different methods (e.g. Knopoff, 1961; Langston and Helmberger, 1975; Dziewonski et al., 1981).

In parallel with the development of the modern seismology, the theory of Plate Tectonics changed the way geologists understand the Earth. Since the end of the 16th century naturalists made observations on the potential continental drifting; but it was in the early 20th century when the theory started to be formally proposed (Taylor, 1910; Wegener, 1912; Schwinner, 1919; Holmes, 1931). The relevant information acquired on the magnetic stripes on the ocean floor in the 60's (e.g. Hess, 1962; Vine, 1966; Le Pichon, 1968; Morgan, 1968), in addition to an increasing number of geological and geophysical observations, established the Plate Tectonics as the global geodynamical paradigm on Earth Sciences. The study of earthquakes related to Plate Tectonics was developed at the same time establishing the basic concepts of seismotectonics and the lithospheric deformation (e.g. Benioff, 1954; Sykes, 1967; Isacks et al., 1968; Isacks and Molnar, 1969).

Since the 70's focal mechanisms are computed in a systematic way and global catalogs of focal mechanisms are available since then. As the amount of data increases, our knowledge on the active tectonics improves. As a consequence of the continuous increase of data available we need new tools to analyze it systematically.

In order to represent focal mechanism populations Frohlich and Apperson (1992) proposed a diagram to visualize focal mechanism data as a function of the rupture type. This kind of representation is popular and widely used on seismotectonics to represent the focal mechanism types of the study areas (e.g. Frohlich et al., 1997; Borges et al., 2001; Igarashi et al., 2001; Ratchkovski and Hansen, 2002; Kita et al., 2006; Serpelloni et al., 2007). This

representation is not accurate, presenting distortion problems (Frohlich, 2001), and Kagan (2005) used the Kaverina et al. (1996) projection to avoid them. The latter projection is used in `FMC` by default.

7 The focal mechanism

The term "focal mechanism" is used to refer to the parameters that characterize an earthquake rupture. A focal mechanism usually presents the characteristics of the two orthogonal possible rupture planes: strike, dip and rake of the slip vector over the plane. The energy released by the event, its hypocentral location and the exact time of occurrence are also given. The focal mechanism can, instead of describe the geometry of the possible rupture planes (6 variables), describe the characteristics of the rupture by means of the seismic moment tensor (SMT) or centroid moment tensor (CMT) (6 variables).

The SMT is based in the representation of the equivalent forces on a point seismic source. In this tensor the sum of angular moments should be null, in other words, the SMT is a symmetric tensor on a three dimensional space (9 components) with 6 independent components:

$$\boldsymbol{M} = \begin{pmatrix} M_{XX} & M_{XY} & M_{XZ} \\ M_{YX} & M_{YY} & M_{YZ} \\ M_{ZX} & M_{ZY} & M_{ZZ} \end{pmatrix} \tag{7.1}$$

where

$$\begin{aligned} M_{XY} &= M_{YX} \\ M_{XZ} &= M_{ZX} \\ M_{YZ} &= M_{ZY} \end{aligned} \tag{7.2}$$

Similarly to the strain tensor where we can define the orientation of the principal axes (eigenvectors) and its magnitudes (eigenvalues), the SMT can be defined by the orientation of its principal axes P, B and T (eigenvectors) and its magnitudes (eigenvalues). The T axis describes the greatest of the eigenvalues, the P describes the lowest and the B the intermediate.

If the seismic event is generated by the slip in a fault rupture, its characteristics should be well described as a double couple moment tensor (Figure 7.1):

$$\boldsymbol{M} = \begin{bmatrix} M_0 & 0 & 0 \\ 0 & -M_0 & 0 \\ 0 & 0 & 0 \end{bmatrix} \tag{7.3}$$
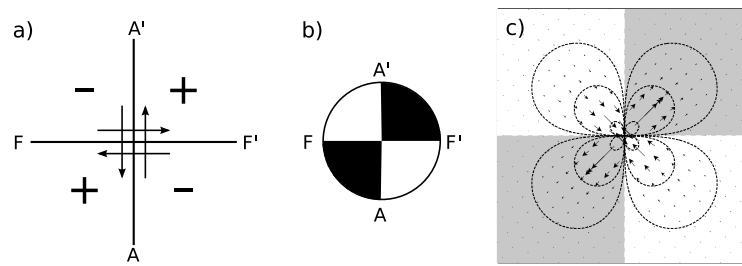
Figure 7.1: Double couple deformation mechanism. a) Plan view of horizontal displacement on an idealized point vertical fault A-A' or F-F' and resulting distribution of compressions (+) and dilatations (-). b) Focal mechanism representation on a stereographic projection. Compression quadrants are filled. c) Horizontal displacement produced by a point size vertical dislocation computed with the Okada (1992) equations; compressional quadrants are filled while dilatational are kept empty following the focal mechanism representation. a) and b) modified from Bullen and Bolt (1985).

where M_0 is the scalar seismic moment.

The most used representation of the double couple is based on the stereographic projection. In this projection both nodal planes of the focal mechanism are plotted, and the quadrants containing the T axis, the compression quadrants, are filled (Figure 7.1). This kind of representation - commonly called "beach-ball" - located on a map on the earthquake epicenter is useful to interpret the seismic data from a tectonic point of view, allowing the study of the earthquake and its rupture fault plane on its tectonic context, being one of the basis of the seismotectonics. The compressional and dilatational quadrants are separated by two orthogonal planes, the nodal planes, being one of them the plane of rupture that generated the earthquake (Figure 7.2).

As we increase the number of focal mechanisms to study, we increase the difficulty to interpret the data, obscuring frequently the details of a tectonic environment if we just project them over a map. In order to facilitate the study of groups of focal mechanisms several plots can be proposed, great part of them based on classical structural geology plots.

The plots inherited from the structural geology are based in the geometrical characteristics of the nodal planes of the SMT, equivalent to the characteristics of the fault planes: strike (φ), dip (δ) and rake (λ) (Figure 7.2). The main problem of these representations is the duplication of data. Each focal mechanism presents two equivalent and orthogonal nodal planes. The selection of one of them as the fault plane is not straightforward and although from a mechanical point of view they can be discriminated (McKenzie, 1969; Michael, 1987; Gephart, 1990), when both nodal planes are me-
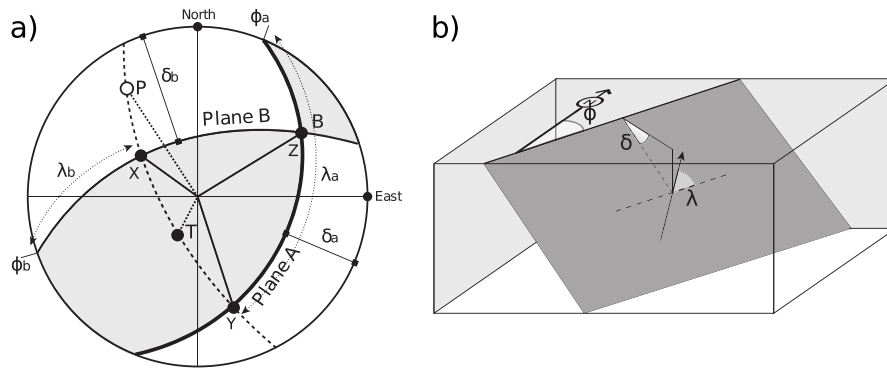
Figure 7.2: a) Focal sphere diagram on stereographic projection on the lower hemisphere. Nodal planes A and B, A representing the fault plane and B the auxiliary plane, with its orientation characteristics: φ, strike; δ, dip and λ, rake. The orientation of the SMT principal axes are also shown: T, B and P. Modified from Udías (1989). b) Block diagram showing the parameters that define the orientation of a fault plane in the space: φ, strike; δ, dip and λ, rake.

chanically compatible or reactivated structures can be present, additional geological and/or geophysical information is required. There are as many representations of this kind as possible combinations between these parameters and its derivatives (usually trigonometrical functions). These relations can be represented in biaxial plots or stereographic projections (e.g. Davis and Reynolds, 1996; Ramsay and Huber, 1997; Pollard and Fletcher, 2005).

The focal mechanisms can also be plotted as function of the principal axes T, B and P. These axes form an orthogonal system. The orientation of each axis can be defined in the space as any line, by its direction and plunge. The main advantages of these representations are: the univocality, each focal mechanism is represented by one point; its simplicity of interpretation, the kind of deformation (normal, reverse, strike-slip) is function of the plunge of the axes; and the reduction of errors compared with the planes, as they are derived from the principal axes of the SMT (Vannucci and Gasperini, 2003).

8 Diagram

Frohlich and Apperson (1992) developed a ternary diagram to represent focal mechanisms based in the trigonometrical relation:

$$\sin^2 \iota_T + \sin^2 \iota_B + \sin^2 \iota_P = 1, \qquad (8.1)$$

where ι_T, ι_B and ι_P are the plunges of the axis T, B and P of the SMT. This relation is true for three orthogonal axes.

As the equation of a sphere with radius unity is

$$x^2 + y^2 + z^2 = 1 \tag{8.2}$$

and all the plunge angles are positive between 0°and 90°, then the representation of a focal mechanism defined by these axes is equivalent to the projection of a point in an spherical octant over a planar surface. As a sphere is not a developable surface can not be projected onto a plane without distortion.

The projection used by Frohlich and Apperson (1992) represents this spherical octant as a triangle, which is equivalent to the gnomonic geographical projection. In this projection we define the angles

$$\psi = \arctan\left(\frac{\sin \iota_T}{\sin \iota_P}\right) - 45°, \tag{8.3}$$

and

$$\iota_s = \arcsin\frac{1}{\sqrt{3}} = \arctan\frac{1}{\sqrt{2}} \approx 35.26°, \tag{8.4}$$

which is the angle of the ternary symmetry axis with the orthogonal axes of the octant.

From these angles the x and y coordinates over the plane are given by:

$$x = \frac{\cos \iota_B \cdot \sin \psi}{\sin \iota_s \cdot \sin \iota_B + \cos \iota_s \cdot \sin \iota_B \cdot \cos \psi} \tag{8.5}$$

$$y = \frac{\cos \iota_s \cdot \sin \iota_B - \sin \iota_s \cdot \cos \iota_B \cdot \cos \psi}{\sin \iota_s \cdot \sin \iota_B + \cos \iota_s \cdot \sin \iota_B \cdot \cos \psi} \tag{8.6}$$

The angle ι_s in the projection is the angle of the plunges of the axes T, B and P for the focal mechanism that occupies the barycentre of the ternary diagram where $x = y = 0$.

As can be seen in Figure 8.1a this projection introduces remarkable distortions towards the extremes of the diagram. This distortions could difficult the study of some groups of focal mechanisms as the author pointed out (Frohlich, 2001). In order to avoid these distortions Kaverina et al. (1996) proposed the use of a projection capable of maintain the proportion of the areas equal, equivalent to the Lambert azimuthal equal-area projection (Figure 8.1b), which is the used in structural geology to generate the stereographic equal-area Schmidt stereonet. In this case the limits of the diagram are formed by great circles instead of straight lines forming a triangle (Figure 8.1).
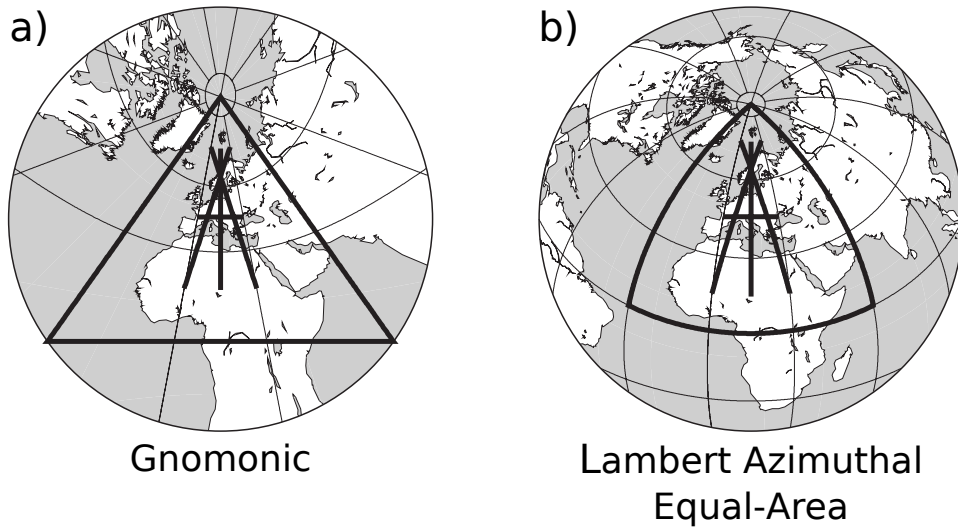
Figure 8.1: Representation of an hemisphere of the globe centred on Europe (45°N, 15°E) in the two different projections referenced in the text: a) Gnomonic projection; b) Lambert azimuthal equal-area. In thick lines are marked the spheric octant and some reference lines in order to compare both projections.

If we take the sines of the plunges of the main axes ι_T, ι_B and ι_P:

$$z_T = \sin \iota_T$$
$$z_P = \sin \iota_P \tag{8.7}$$
$$z_B = \sin \iota_B$$

the length of the vector that connects the center of the diagram with the projected point is defined by

$$L = 2 \sin \left[\frac{1}{2} \cdot \arccos \left(\frac{z_T + z_P + z_B}{\sqrt{3}} \right) \right] \tag{8.8}$$

and the normalization factor is:

$$N = \sqrt{2 \cdot [(z_B - z_P)^2 + (z_B - z_T)^2 + (z_T - z_P)^2]} \tag{8.9}$$

The coordinates of the projected focal mechanisms in the plane are defined as follows (these equations corrects the wrong equations showed in Kagan (2005)):

$$x = \sqrt{3} \cdot \frac{L}{N} \cdot (z_P - z_T)$$
$$y = \frac{L}{N} \cdot (2z_B - z_P - z_T) \tag{8.10}$$

9   Focal Mechanism Classification

In order to classify the focal mechanisms Kagan (2005) divided the octant in three areas (Figure 9.1b) corresponding to the three basic Andersonian regimes: normal, reverse and strike-slip. The dividing lines start at the diagram center and run through the middle of each great circle (dashed lines in Figure 9.1b). This classification, although simple and straightforward, is too basic sometimes for a detailed seismotectonic study.
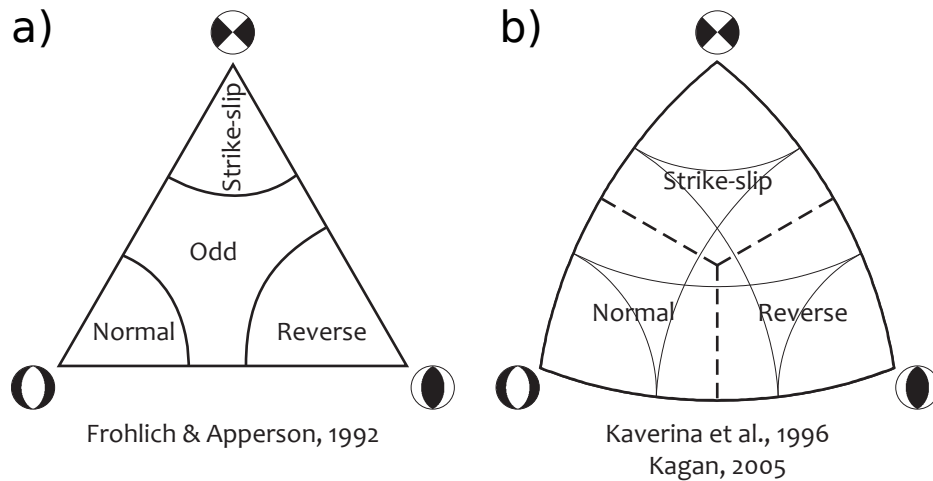

Figure 9.1: Focal mechanisms classification diagrams based on SMT axes plunges proposed by a) Frohlich and Apperson (1992) and b) Kagan (2005).

From the seismotectonic point of view an earthquake reflects the brittle lithospheric strain produced by tectonic processes. The vast majority of earthquakes are produced by displacements on faults (some other processes as deep volume changes or cave collapses can produce seismic signals too), and they are interpreted usually as fault ruptures. Following this reasoning the most appropriate classification for the focal mechanism should be done by means of the slip vector on the fault, given by the rake angle. This classification can be done following one of the proposed conventions (Rickard, 1972; Aki and Richards, 1980; Angelier, 1994). As has been mentioned before, the problem is the duplicity of data due to the two nodal planes solution of the focal mechanism.
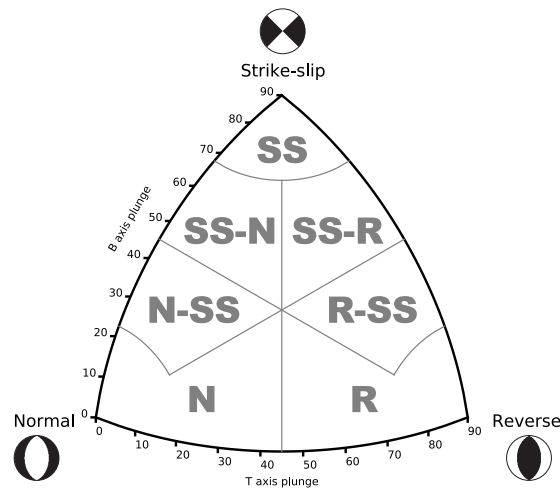
Figure 9.2: Focal mechanism classification diagram. N) Normal; N-SS) Normal - Strike-slip; SS-N) Strike-slip - Normal; SS) Strike-slip; SS-R) Strike-slip - Reverse; R-SS) Reverse - strike-slip and R) Reverse.

An extended discussion on the relation among the different focal mechanism parameters can be found on Célérier (2010); the author also points out the difficulty on interpreting the stress state from the focal mechanisms, specially where oblique faulting takes place and reactivation of inherited structures is possible (Wyss et al., 1992).

However the SMT can be interpreted as a seismic strain tensor (Kostrov, 1974) where the main axes are equivalent to the SMT main axes (Wyss et al., 1992). With this relation in mind we can interpret the populations of focal mechanisms as representations of strains in different tectonic settings. Oblique slip focal mechanisms with normal component can be interpreted as transtensional strain, while oblique slip focal mechanisms with reverse component can be interpreted as transpressional.

In order to count with a classification more detailed than the one of Kagan (2005) I decided to classify the focal mechanism in a series of fields that include the oblique slip regimes (Álvarez-Gómez, 2009). This approximation is similar to the Johnston et al. (1994) classification; with 7 classes of earthquakes: 1) Normal; 2) Normal - Strike-slip; 3) Strike-slip - Normal; 4) Strike-slip; 5) Strike-slip - Reverse; 6) Reverse - Strike-slip and 7) Reverse. The resulting diagram incorporating this 7 fields classification to the Kaverina projection is shown in Figure 9.2.

The algorithm to classify the focal mechanisms based on the SMT main axes plunges is the shown in Figure 4.1.

When one of the three main SMT axes is greater or equal than $67.5°$ (resulted from $3 * \frac{\pi/2}{4}$) we obtain a "pure" Andersonian tectonic regime. From
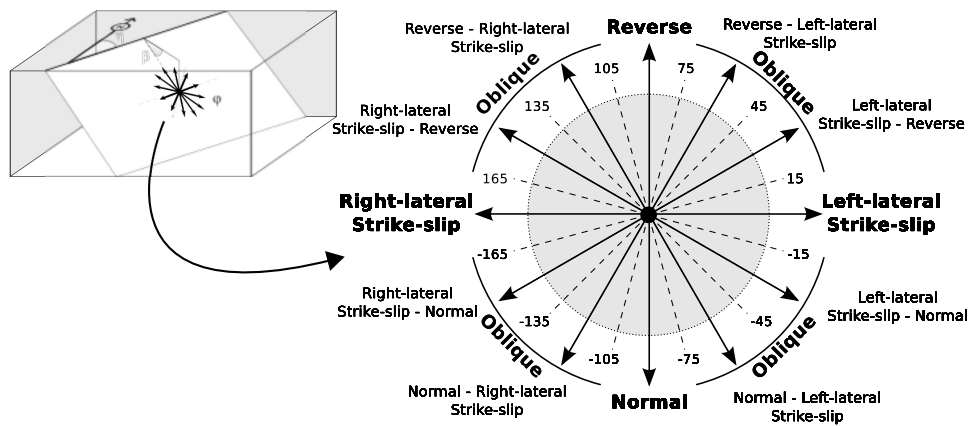
Figure 9.3: Diagram showing the convention used in this work for the rake classification of faults or focal mechanism nodal planes. Inside the grey circle the equivalent SMT axes-based classification is shown (Figure 8.1).

the pure normal or reverse faulting to the strike-slip faulting there is a range of oblique faulting types with more or less relevance of the horizontal component. On the other hand between the pure normal and pure reverse faulting there is a permutation of the T and P axes in the vertical position, while the B axis remains horizontal. The transition takes place when the P and T axes plunge equally and a vertical nodal plane is present.

In the following section I compare the results of both classifications, the one based in the main axes plunges of the moment tensor and the one based on the fault rakes.

9.1 Comparison between rake-based and SMT axes-based classifications

In order to classify the nodal planes according to its rakes I adopted a convention hybrid between the Rickard (1972) and Aki and Richards (1980) conventions. The focal mechanism rakes are usually given with the Aki and Richards (1980) convention, while from a geological point of view the Rickard (1972) convention is more used. I define 7 equivalent classes to those used in the SMT axes-based classifications (Figure 9.3).

Each one of the nodal planes of the focal mechanisms from the Global CMT catalog (Ekström et al., 2012) is classified according to the rake classification shown in Figure 9.3. From the analysis of the focal mechanism alone we cannot choose unequivocally the fault plane responsible of the earthquake. To analyze the degree of uncertainty I show in Figure 9.4a the relative frequency of relations between nodal planes rupture types. For example, it

28

can be seen that when one nodal plane is classified as normal, the other can be normal as well, or can present some strike-slip component, but it can not present reverse component; the same can be said for the reverse nodal planes. When one nodal plane is pure strike-slip, the other can present dip-slip component too, ranging from normal with strike-slip component (N-SS) to reverse with strike-slip component (R-SS), but being more frequent the relations between nodal planes of mainly strike-slip type.

Comparing the focal mechanism classified with the SMT axes and the nodal planes classified with the rakes (Figure 9.4b) a similar picture as the described above can be seen. The percentages of relations change sensibly, but the common picture is the same. When the focal mechanism is classified as normal type we can expect that both nodal planes are of normal type or normal with some strike-slip component. Similarly when the focal mechanism is classified as reverse, both nodal planes are mainly of the reverse type too. For the case of the strike-slip focal mechanism almost all the nodal planes are of strike-slip type too.

We can conclude that there is not much difference between the results obtained from the rake classification of the nodal planes and the classification of the focal mechanism attending to the SMT axes plunges. The focal mechanism classification based on the SMT axes has the advantage of the univocallity of its classification, in contrast with the duplicity of data and uncertainty related to the nodal planes rake classification.

a) Nodal Plane A class

	N	N-SS	SS-N	SS	SS-R	R-SS	R
N	7.7						
N-SS	4.2	6.8					
SS-N	0.9	4.6	3.1				
SS	0.4	1.5	5.8	11.1	5.1	1.7	0.3
SS-R					3.1	6.2	1.2
R-SS						8.9	11.3
R							16.1

Nodal Plane B class

b) Focal Mechanism class

	N	N-SS	SS-N	SS	SS-R	R-SS	R
N	10.5						
N-SS	7.2	4.4	0.3				
SS-N	1.1	2.1	4.3	1.2			
SS	0.6	0.2	2.0	13.2	1.8	0.2	0.6
SS-R				1.0	4.0	2.7	1.7
R-SS					0.3	5.5	12.7
R							22.6

Nodal Planes class
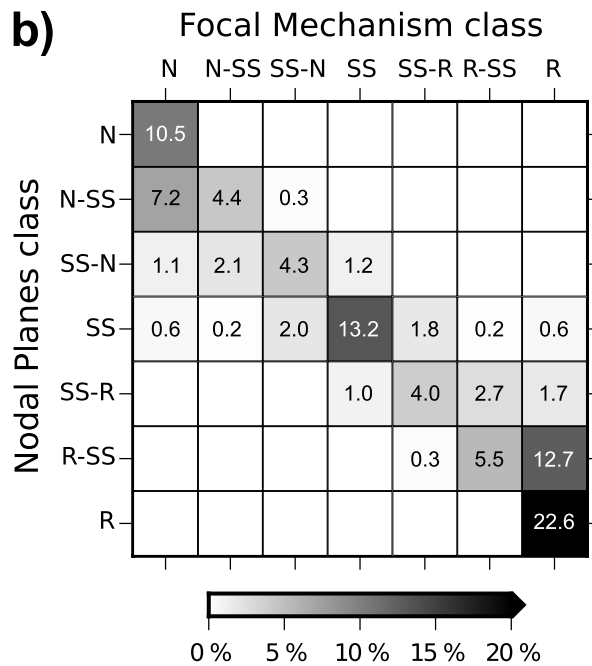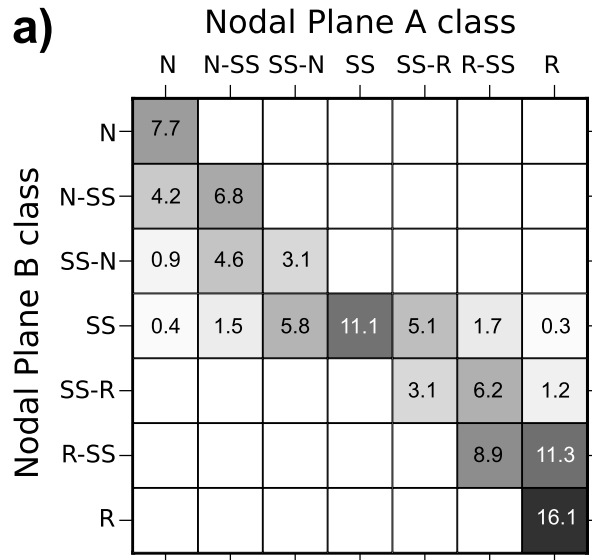
0 % 5 % 10 % 15 % 20 %

Figure 9.4: Heatmaps of the proportion of relations between a) both nodal planes rupture type based on the rake classification, and b) between the focal mechanism classification and the nodal planes rupture types rake classification. The data used is the entire Global CMT catalog (Ekström et al., 2012). Numbers show percentages over the entire catalogue.

References

Aki, K., Richards, P., 1980. Quantitative Seismology, Theory and Methods, Vol. I and II. W.H. Freeman, San Francisco.

Álvarez-Gómez, J. A., 2009. Tectónica Activa y Geodinámica en el Norte de Centroamérica. Ph.D. thesis, Universidad Complutense de Madrid, Madrid.

Angelier, J., 1994. Palaeostress analysis of small-scale brittle structures. In: Hancock, P. (Ed.), Continental Deformation. Pergamon Press Ltd, p. 421.

Benioff, H., 1954. Orogenesis and Deep Crustal Structure-Additional Evidence from Seismology. Geological Society of America Bulletin 65 (5), 385–400.

Borges, J. F., Fitas, A. J., Bezzeghoud, M., Teves-Costa, P., 2001. Seismotectonics of Portugal and its adjacent Atlantic area. Tectonophysics 331 (4), 373–387.

Bullen, K. E., Bolt, B. A., 1985. An introduction to the theory of seismology, 4 Edition. Cambridge University Press, Cambridge.

Byerly, P., 1928. The nature of the first motion in the Chilean earthquake of November 11, 1922. American Journal of Science Series 5 Vol. 16 (93), 232–236.

Byerly, P., 1938. The earthquake of July 6, 1934: Amplitudes and First Motion. Bulletin of the Seismological Society of America 28 (1), 1–13.

Célérier, B., 2010. Remarks on the relationship between the tectonic regime, the rake of the slip vectors, the dip of the nodal planes, and the plunges of the P, B, and T axes of earthquake focal mechanisms. Tectonophysics 482 (1–4), 42–49.

Davis, G. H., Reynolds, S. J., 1996. Structural geology of rocks and regions, 2 Edition. Willey, New York.

Dziewonski, A. M., Chou, T.-A., Woodhouse, J. H., 1981. Determination of earthquake source parameters from waveform data for studies of global and regional seismicity. Journal of Geophysical Research: Solid Earth 86 (B4), 2825–2852.

Ekström, G., Nettles, M., Dziewoński, A., 2012. The global CMT project 2004-2010: Centroid-moment tensors for 13,017 earthquakes. Physics of the Earth and Planetary Interiors 200-201 (0), 1–9.

Frohlich, C., 2001. Display and quantitative assessment of distributions of earthquake focal mechanisms. Geophysical Journal International 144 (2), 300–308.

Frohlich, C., Apperson, K. D., 1992. Earthquake focal mechanisms, moment tensors, and the consistency of seismic activity near plate boundaries. Tectonics 11 (2), 279–296.

Frohlich, C., Coffin, M. F., Massell, C., Mann, P., Schuur, C. L., Davis, S. D., Jones, T., Karner, G., 1997. Constraints on Macquarie Ridge tectonics provided by Harvard focal mechanisms and teleseismic earthquake locations. Journal of Geophysical Research: Solid Earth (1978–2012) 102 (B3), 5029–5041.

Gasperini, P., Vannucci, G., 2003. FPSPACK: a package of FORTRAN subroutines to manage earthquake focal mechanism data. Computers & Geosciences 29 (7), 893–901.

Gephart, J. W., 1990. Stress and the direction of slip on fault planes. Tectonics 9 (4), 845–858.

Hess, H. H., 1962. History of ocean basins. Petrologic studies 4, 599–620.

Holmes, A., 1931. Radioactivity and earth movements. Nature 128, 496.

Honda, H., Masatuke, A., 1952. On the Mechanism of the Earthquakes and the Stresses Producing Them in Japan and Its Vicinity. Science Reports Tohoku University 4 (1).

Igarashi, T., Matsuzawa, T., Umino, N., Hasegawa, A., 2001. Spatial distribution of focal mechanisms for interplate and intraplate earthquakes associated with the subducting Pacific plate beneath the northeastern Japan arc: A triple-planed deep seismic zone. Journal of Geophysical Research: Solid Earth (1978–2012) 106 (B2), 2177–2191.

Isacks, B., Molnar, P., 1969. Mantle earthquake mechanisms and the sinking of the lithosphere. Nature 223 (5211), 1121–1124.

Isacks, B., Oliver, J., Sykes, L. R., 1968. Seismology and the new global tectonics. Journal of Geophysical Research 73 (18), 5855–5899.

Johnston, A. C., Coppersmith, K. J., Kanter, L. R., Cornell, C. A., 1994. The earthquakes of stable continental regions. Volume 1: Assessment of large earthquake potential. Tech. rep.

Kagan, Y. Y., 2005. Double-couple earthquake focal mechanism: random rotation and display. Geophysical Journal International 163, 1065–1072.

Kaverina, A. N., Lander, A. V., Prozorov, A. G., 1996. Global creepex distribution and its relation to earthquake-source geometry and tectonic origin. Geophysical Journal International 125 (1), 249–265.

Kita, S., Okada, T., Nakajima, J., Matsuzawa, T., Hasegawa, A., 2006. Existence of a seismic belt in the upper plane of the double seismic zone extending in the along-arc direction at depths of 70–100 km beneath NE Japan. Geophysical Research Letters 33 (24).

Knopoff, L., 1961. Analytical calculation of the fault-plane problem. Publications of the Dominion Observatory (Ottawa) 24, 309–315.

Koning, L. P. G., 1941. On the Mechanism of Deep Focus Earthquakes. Gerlands Beitrage z. Geophysik 58, 159–197.

Kostrov, V., 1974. Seismic moment and energy of earthquakes, and seismic flow of rock. Izv. Earth Phys. 1, 23–40 (translation UDC 550.341, pp13–21).

Langston, C. A., Helmberger, D. V., 1975. A procedure for modelling shallow dislocation sources*. Geophysical Journal of the Royal Astronomical Society 42 (1), 117–130.

Le Pichon, X., 1968. Sea-floor spreading and continental drift. Journal of Geophysical Research 73 (12), 3661–3697.

McKenzie, D. P., 1969. The relation between fault plane solutions for earthquakes and the directions of the principal stresses. Bulletin of the Seismological Society of America 59 (2), 591–601.

Michael, A. J., 1987. Use of focal mechanisms to determine stress: a control study. Journal of Geophysical Research 92 (B1), 357–368.

Morgan, W. J., 1968. Rises, trenches, great faults, and crustal blocks. Journal of Geophysical Research 73 (6), 1959–1982.

Okada, Y., 1992. Internal deformation due to shear and tensile faults in a half-space. Bulletin of the Seismological Society of America 82 (2), 1018–1040.

Pollard, D. D., Fletcher, R. C., 2005. Fundamentals of Structural Geology, 1 Edition. Cambridge University Press, Cambridge.

Ramsay, J. G., Huber, M. I., 1997. The Techniques of Modern Structural Geology, Vol 2: Folds and Fractures, 5 Edition. Academic Press, London.

Ratchkovski, N. A., Hansen, R. A., 2002. New evidence for segmentation of the Alaska subduction zone. Bulletin of the Seismological Society of America 92 (5), 1754–1765.

Rickard, M. J., 1972. Fault Classification: Discussion. Geological Society of America Bulletin 83 (8), 2545–2546.

Scheidegger, A. E., 1957. The geometrical representation of fault-plane solutions of earthquakes. Bulletin of the Seismological Society of America 47 (2), 89–110.

Scholz, C. H., 2002. The mechanics of earthquakes and faulting, 2nd Edition. Cambridge University Press, Cambridge.

Schwinner, R., 1919. Vulkanismus und Gebirgsbildung: ein Versuch. Reimer.

Serpelloni, E., Vannucci, G., Pondrelli, S., Argnani, A., Casula, G., Anzidei, M., Baldi, P., Gasperini, P., 2007. Kinematics of the Western Africa-Eurasia plate boundary from focal mechanisms and GPS data. Geophysical Journal International 169, 1180–1200.

Sykes, L. R., 1967. Mechanism of earthquakes and nature of faulting on the Mid-Oceanic Ridges. Journal of Geophysical Research 72 (8), 2131–2153.

Taylor, F. B., 1910. Bearing of the tertiary mountain belt on the origin of the earth's plan. Geological Society of America bulletin 21, 179–226.

Udías, A., 1989. Parámetros del foco de los terremotos. Física de la Tierra 1, 87–104.

Vannucci, G., Gasperini, P., 2003. A database of revised fault plane solutions for Italy and surrounding regions. Computers & Geosciences 29 (7), 903–909.

Vine, F. J., 1966. Spreading of the ocean floor: New evidence. Science 154 (3755), 1405–1415.

Wegener, A., 1912. Die Entstehung der Kontinente. Geologische Rundschau 3 (4), 276–292.

Wessel, P., Smith, W. H. F., Scharroo, R., Luis, J. F., Wobbe, F., 2013. Generic Mapping Tools: Improved version released. EOS Transactions of the American Geophysical Union 94, 409–410.

Wyss, M., Liang, B., Tanigawa, W. R., Wu, X., 1992. Comparison of orientations of stress and strain tensors based on fault plane solutions in Kaoiki, Hawaii. Journal of Geophysical Research 97 (B4), 4769–4790.